

Original paper

Late Ordovician magmatic pulse in the Tugrug Group, the Gobi Altai Zone, SW Mongolia

Pavel HANŽL^{1*}, Lucie UHROVÁ¹, Kristýna HRDLIČKOVÁ¹, Karel SCHULMANN¹,
David BURIÁNEK¹, Orgil GANSUKH², Jitka MÍKOVÁ¹

¹ Czech Geological Survey, Klárov 3, 118 21 Prague 1, Czech Republic; pavel.hanzl@geology.cz

² Geological Institute MAS, Songinokhairkhan district, 19th khoroo, 3rd building, Ulaanbaatar

*Corresponding author



The Mongolian Altai Domain of the Central Asian Orogenic Belt is formed by a giant Lower Palaeozoic accretionary wedge that was later thrust over the northerly Central Mongolian Microcontinent. This accretionary complex mainly consists of late Cambrian–Ordovician volcano–sedimentary rocks represented by various formations within the Tugrug Group which were deformed, metamorphosed and intruded by numerous plutons during the Devonian–Carboniferous orogenic events. In this work, we report new U–Pb zircon ages of two felsic igneous rocks indicating an existence of the so far neglected late Ordovician magmatic event affecting the Mongolian Altai accretionary wedge. The felsic volcanic sheet inside the upper part of the Tugrug Group in the western Gobi Altai Zone (eastern part of the Mongolian Altai Domain) yields an age of 457 ± 2 Ma and nearby granite pluton intruding the entire volcano–sedimentary sequence gives an age of 445 ± 1 Ma. Both rocks are high-K calc-alkaline, peraluminous, with similar geochemical patterns characterised by enrichment in mobile lithophile elements over Nb, Ti, P and Sr and nearly identical REE trends. All together, these features point to an analogous volcanic–arc-related magma source. This magmatism reflecting terminal stages of the accretionary wedge formation in the Mongolian Altai Domain may be related to the recently proposed late Ordovician orogenic event.

Keywords: Mongolian Altai accretionary wedge, Tugrug Group, Ordovician magmatism, zircon dating

Received: 19 June 2023; **accepted:** 23 November 2023; **handling editor:** V. Janoušek

The online version of this article (doi: 10.3190/jgeosci.385) contains electronic supplementary material.

1. Introduction

The topography of the Gobi and Mongolian Altai Mountain chains in southwestern Mongolia have risen due to the intracontinental deformation along restraining bands of the major Cenozoic strike-slip faults (Cunningham and Dickinson 2006). These ranges uncover representative geological exposures allowing to explore in detail Palaeozoic architecture of the critical units forming the so-called Mongolian collage (Xiao et al. 2015), which is a part of the Central Asian Orogenic Belt (CAOB, Fig. 1a) (Mossakovsky et al. 1993) known also as the Altaid supercollage (Xiao et al. 2015, 2018). A string of the Tuva, Zavkhan and Baidrag Precambrian continental blocks constituting the Central Mongolian Microcontinent (CMM of Tomurtogoo 2014) in the core of the Mongolian collage were amalgamated to the Siberia margin during the late Proterozoic to Cambrian orogenic event (e.g., Şengör et al. 1993; Khain et al. 2003; Cocks and Torsvik, 2007). In Mongolia, this event started by early Cambrian thrusting of Neoproterozoic ophiolites over the southern margin of the Baidrag and Zavkhan blocks (e.g., Dijkstra et al. 2006; Bold et al. 2016; Buriánek et al. 2017). The stacked nappes, together with the underlying base-

ment, were subsequently intruded by mid-Cambrian to early Ordovician Ikh-Mongol magmatic arc that evolved above a north-east dipping (in present-day coordinates) subduction zone (Janoušek et al. 2018). The intrusion of arc magmas was accompanied by the development of a giant accretionary volcano–sedimentary wedge forming the bulk of the Mongolian Altai Mountain range (e.g., Xiao et al. 2004; Windley et al. 2007; Jiang et al. 2017). The Lower Palaeozoic turbiditic and volcano–sedimentary sequences of this Mongolian Altai accretionary wedge (MAW) extend for two thousand kilometres from the Gobi Altai in the southeast Mongolia, via Chinese to Gorny Altai in the northwest (e.g., Xiao et al. 2009). The MAW developed in front of the Pacific type subduction zone during its *c.* 200 My long history (e.g., Jiang et al. 2017).

Buriánek et al. (2022) described three early to middle Palaeozoic evolutionary stages forming the MAW structure: 1) Cambrian–Ordovician deposition of volcano–sedimentary sequences due to 60 My long subduction roll-back; 2) late Ordovician–Silurian volcanic gap associated with Barrovian metamorphism and thickening of the wedge due to switch to advancing subduction mode (Soejono et al. 2021); 3) early to mid-Devonian melting

and extensional thinning of the wedge interpreted to result from renewed subduction roll-back (Buriánek et al. 2022; Sukhbaatar et al. 2022).

So far, there have been only a few late Ordovician intrusions reported in the MAW, mainly in the Chinese Altai (Broussolle et al. 2019 for review), in the Khovd Zone (Soejono et al. 2016) or in the Gobi Altai Zone (Kröner et al. 2010). These relatively rare I- to S-type granitoids are traditionally interpreted as a result of syn-subduction magmatism (Wang et al. 2006; Yuan et al. 2007; Sun et al. 2008; Cai et al. 2011). The presence of this magmatism is undervalued in the current literature, and its geodynamic significance is poorly understood.

In this contribution, we present new LA-ICP-MS zircon U–Pb ages and whole-rock geochemistry from the granite and rhyolite belonging to the weakly metamorphosed upper part of the Cambrian–Ordovician volcano-sedimentary Tugrug Group in the Ar Dalangiin Range (northwestern part of the Gobi Altai Zone). These rocks yielded surprising late Ordovician zircon U–Pb ages that can be regarded as an important marker of tectonothermal and possibly syn-sedimentary magmatic history of the Mongolian Altai Domain. An attempt is made to attribute this specific magmatic event to the terminal stage of sedimentary evolution of the MAW hallmarking transition to syn-orogenic magmatism in the frame of the recently proposed model of Buriánek et al. (2022).

2. Geological setting

2.1. Regional overview

Geological units of southwestern Mongolia (Fig. 1b) south of the Zavkhan–Baidrag Precambrian blocks of the CMM have been traditionally assigned to numerous terranes representing former arcs, back-arcs, metamorphic and accretionary wedges (Badarch et al. 2002). However, in this study we prefer to use a simple division of this part of the Mongolian Collage into three parallel tectonic domains as defined by Kröner et al. (2010): the Lake Zone in the north, the Mongolian Altai in the centre and the Trans-Altai in the south. The northerly Lake Zone represents the Ediacaran–Cambrian oceanic island-arc system with common ophiolite fragments thrust over CMM and intruded by mid-Cambrian–early Ordovician arc-type plutons (e.g., Khain et al. 2003; Jian et al. 2014; Buriánek et al. 2017; Khukhuudei et al. 2022). The original boundary with the southerly Mongolian Altai Domain was reworked by a system of Cenozoic faults known as the Main Mongolian Lineament (Badarch et al. 2002; Tomurtogoo 2014). Palaeozoic volcano-sedimentary units and metamorphic complexes of the Mongolian Altai Domain are separated from the southerly Trans-Altai

Domain by the Cenozoic Bulgan and Trans-Altai faults. Sequences of the Devonian and Carboniferous volcanic arcs alternating with the late Cambrian to Devonian ophiolitic rocks are characteristic of the Trans-Altai Domain (Ruzhentsev et al. 1985; Ruzhentsev and Pospelov 1992; Helo et al. 2006; Lehmann et al. 2010; Jian et al. 2014; Nguyen et al. 2018).

Massive production of plutonic rocks with significant mantle or juvenile component is typical of the evolution of the whole CAO (Jahn et al. 2000). While Cambrian–early Ordovician arc-type gabbros, diorites and granodiorites are generally restricted to the Lake Zone (e.g., Janoušek et al. 2018), mainly Devonian to Permian–Triassic magmatic events are known from the MAW (Cai et al. 2015). Finally, Carboniferous arc granite and granodiorite to post-tectonic Permian alkaline feldspar granite are characteristic of the Trans-Altai Domain (see Hanžl et al. 2023 for review). Altogether, the younging of the magmatism from the north to the south was previously interpreted as a result of continuous migration of arc magmatic front related to the roll-back of the subduction system (e.g., Nguyen et al. 2018; Hanžl et al. 2023).

2.2. Volcano-sedimentary sequences of the Mongolian Altai Domain

The Mongolian Altai Domain (Fig. 1b) is further subdivided to the northerly Khovd Zone, the south-westerly Altai Zone and the easterly Gobi Altai Zone (Badarch et al. 2002; Soejono et al. 2017; Buriánek et al. 2022). Metamorphic rocks of the Bodonch–Tseel Zone (Bibikova et al. 1992; Tomurtogoo 2017) are exposed along the southern parts of the Altai and Gobi-Altai zones.

The Cambrian–Ordovician volcano-sedimentary complex of the Khovd Zone was interpreted as a turbidite accretionary wedge (Badarch et al. 2002) with fragments of juvenile continental arc system (Soejono et al. 2016; Buriánek et al. 2022). The Altai Zone is a thick terrigenous sequence deposited between the late Silurian and early Devonian (Long et al. 2019; Khukhuudei et al. 2022). Complex assemblage of the Gobi Altai Zone is built up by volcano-sedimentary sequences of Cambrian to Carboniferous ages (Hanžl et al. 2020) interpreted as a back-arc/forearc system (Badarch et al. 2002). The Bodonch–Tseel Zone was originally described as a basement terrane (Badarch et al. 2002) but it was shown that it represents a metamorphosed equivalent of the Ordovician to Silurian immature volcano-sedimentary sequence (Sukhbaatar et al. 2022).

Recent lithostratigraphic analysis of Buriánek et al. (2022) provided more detailed definition of the whole Palaeozoic sequences of the Mongolian Altai Domain. The earliest Tugrug Group (Jiang et al. 2017; Hanžl et al. 2020) is built by weakly metamorphosed immature

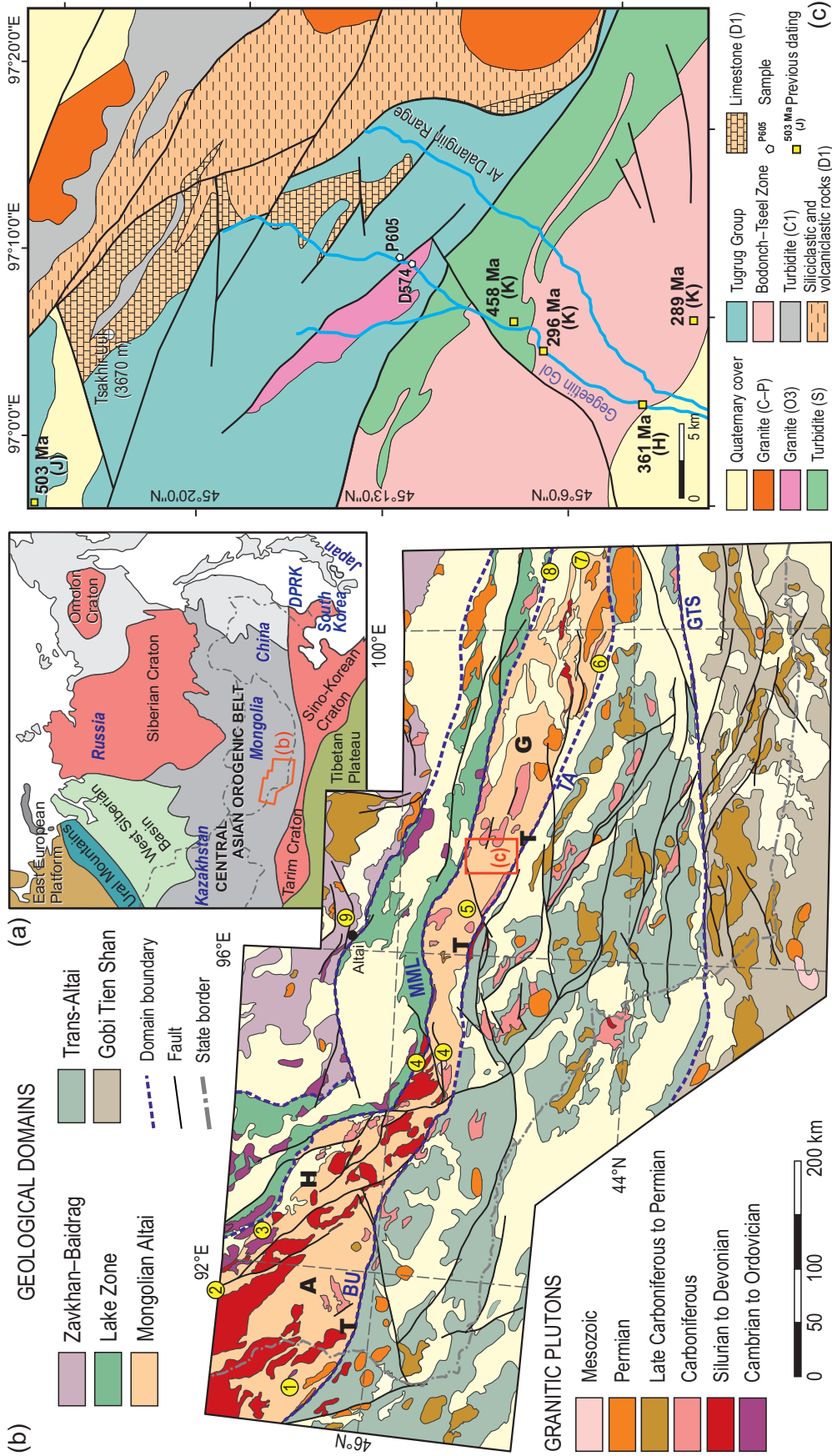


Fig. 1 Geological situation. **a** – Geological position of Mongolia in the frame of CAOB; **b** – Plutonic rocks of the SW Mongolia on the background of the main lithotectonic domains (Kröner et al. 2010; Buriánek et al. 2022) with indication of the Ordovician zircon ages in the Mongolian Altai and adjacent domains. Data sources according to numbers in yellow circles: 1 – Zhang et al. (2017a); 2 – Jiang et al. (2017); Long et al. (2019); 3 – Soejono et al. (2016, 2017); 4 – Sukhbaatar et al. (2022); 5 – Jiang et al. (2017); 6 – Kröner et al. (2010); 7 – Helo et al. (2006); Kröner et al. (2017); 8 – Kröner et al. (2017); 9 – Kozakov et al. (2012). Division of the Mongolian Altai Domain and main faults: A – Altai Zone; H – Khovd Zone; G – Gobi Altai Zone; T – Bodonch-Iseel Zone; BU – Bulgan Fault; TA – Trans Altai Fault; GTS – Gobi Tien Shan Fault; MML – Main Mongolian Lineament. **c** – Geological situation of the Ar Dalangijn Range (modified from Rauzer et al. 1987), with position of studied samples and previous radiometric dating: H – Helo et al. (2006); J – Jiang et al. (2017); K – Kröner et al. (2010).

(flysch-like) sediments containing subalkaline volcanic rocks showing basalt–basaltic andesite and dacite–rhyolite compositional trends (Hanžl et al. 2017). The Tugrug Group includes Tugrug *s.s.* and Ukhinuur formations described by Markova (1975) and Rauzer et al. (1987) in the Gobi Altai Zone and Baatar and Zuunnuruu formations in the Khovd Zone (Buriánek et al. 2022). This volcano-sedimentary sequence represents the dominant lithology of late Cambrian and Ordovician formations in the entire MAW in Mongolia and China, where it is known as the Habahe Group (e.g., Long et al. 2007; Jiang et al. 2011, 2017). The supposed Cambrian–Ordovician age (Borzakovskii 1985) of the sequences was confirmed by detrital zircon age spectra (Jiang et al. 2017; Sukhbaatar et al. 2022).

The following Ordovician Bayantsagaan Formation exposed in the Gobi Altai Zone (Rauzer et al. 1987; Kröner et al. 2010) is dominated by turbiditic sequence of siltstones and sandstones with common volcanogenic admixture and volcanic rocks associated with limestones. The volcano-sedimentary character of the sequence is interpreted as a result of continuous recycling of an active margin with important arc-derived detritus contribution (Buriánek et al. 2022). Ordovician ignimbrite was described from the Botgoniigol Formation of the Khovd Zone, which is an equivalent of the upper part of the Bayantsagaan Formation (Buriánek et al. 2022).

These authors described a hiatus in between the Ordovician Bayantsagaan and Silurian Khutagnuur formations that both consist of siliciclastic flysch-type sediments marking an important volcanic gap. These Silurian sediments were interpreted as mainly proximal deposits of an ocean margin. The overlying Lower–Middle Devonian volcano-sedimentary complexes of the Gichigeny Formation developed as a result of deepening of an extensional basin. Finally, late Devonian shallow-water sediments of the Takhilt Formation were interpreted as a late to post-rift sequence. Local accumulations of the early Carboniferous siliciclastic sediments were described as turbidites of intra-mountain basins (Markova 1975).

The complete lithostratigraphy, palaeontological constraints and U–Pb geochronology of the whole lithostratigraphic column were given in Buriánek et al. (2022), where was also discussed a tectonic significance of individual formations.

The exposures of the igneous and metamorphic rocks along the southern slopes of the Gobi and Mongolian Altai mountain ranges (the Bodonch–Tseel Zone) bear a witness of important Devonian and Permian magmatism and metamorphism (Bibikova et al. 1992; Burenjargal et al. 2016; Khukhudei et al. 2022; Sukhbaatar et al. 2022). This zone has been recently interpreted as a metamorphosed equivalent of the Ordovician to Silurian sequences of the MAW (e.g., Jiang et al. 2017; Sukhbaatar

et al. 2022) partially molten during Devonian and Permian tectono-thermal events (Jiang et al. 2012; Burenjargal et al. 2014; Sukhbaatar et al. 2022).

2.3. Intrusive rocks of the Mongolian Altai Domain

The Mongolian Altai Domain was intruded by numerous granitic plutons related to subduction (e.g., Cai et al. 2015), evolution of metamorphic dome structures (e.g., Lehmann et al. 2010) as well as intra-plate magmatic activity (e.g., Buriánek et al. 2022).

Cai et al. (2015) depicted three phases of plutons emplacement in the Mongolian Altai Domain: middle Palaeozoic (398–350 Ma), late Palaeozoic (317–289 Ma) and Triassic (c. 244–211 Ma). In the Chinese Altai and East Junggar the Palaeozoic granitoid rocks and associated felsic volcanic rocks can be subdivided into as many as nine age populations (Zhang et al. 2017b).

2.3.1. Plutonic rocks of the Altai and Khovd zones

Middle Ordovician gabbro–diorite suite along the north-eastern boundary of the Khovd Zone with the Lake Zone was correlated (Soejono et al. 2016) with the Cambrian–early Ordovician subduction-related gabbros, diorites, quartz diorites and granodiorites of the so-called Ikh-Mongol Arc System (Janoušek et al. 2018 and references therein).

Early Palaeozoic (mainly Devonian) S-type (meta) granites known from the southern part of the Altai Zone (Wang et al. 2006; Yuan et al. 2007; Zhang et al. 2017a) formed coevally with syn-extensional massive anatexis related to LP–HT metamorphism (Burenjargal et al. 2014; Hanžl et al. 2016; Sukhbaatar et al. 2022). Silurian–Devonian and early Carboniferous plutonic rocks in the Chinese and Mongol Altai were originally thought to come from arc-related magmatic source (e.g., Wang et al. 2006; Tong et al. 2012; Cai et al. 2015). However, these granitoids were later reinterpreted to have originated by anatexis of chemically immature metasediments dominated by the Cambrian–Ordovician magmatic arc-derived detritus (e.g., Jiang et al. 2016, 2017). Devonian to early Carboniferous plutons (c. 402–350 Ma) of similar, probably inherited arc signature, occur in western parts of the Mongolian Altai Domain (Cai et al. 2015; Song et al. 2019; Boldbaatar et al. 2021 and references therein). Post-accretionary late Carboniferous to Permian plutons were described mainly from the southern Chinese Altai (e.g., Tong et al. 2014; Cui et al. 2021).

Triassic oval pluton dated by Cai et al. (2015) to 211 ± 2.5 Ma was described from the boundary between

Gobi Altai and Khovd Zone close to the Bugat soum and interpreted as a result of intraplate magmatism. On the other hand, Dash et al. (2016) interpreted peraluminous granites (215 ± 3 Ma) from the western block of the Bodonch–Tseel Zone as related to the crustal thickening.

2.3.2. Plutonic rocks in the Gobi Altai Zone

The age of plutons in the Gobi Altai Zone is less constrained if compared to the western parts of the Mongolian Altai Domain. Granites in the metamorphic complex south of Bayanlig soum were dated as late Silurian (Helo et al. 2006) or as middle Ordovician (Kröner et al. 2017). Devonian plutonic protolith of the orthogneisses (Helo et al. 2006; Demoux et al. 2009; Burenjargal et al. 2014; Hong et al. 2020) common in metamorphic rocks of the Bodonch–Tseel Zone, was interpreted as a product of syn-extensional melting of the wedge sediments and volcanic rocks (Hanžl et al. 2016; Sukhbaatar et al. 2022). On the other hand, early Carboniferous granitoids of the Chandman Massif in the northern Gobi Altai Zone were emplaced in the core of a migmatite–granite dome marking regional compression (Broussolle et al. 2015; Lehmann et al. 2017). In contrary, Hong et al. (2020) interpreted late Carboniferous (303–298 Ma) plutons and rhyolites on the southern slopes of the Gichigeny Range east of our studied valley as A_2 type granites related to the extensional back-arc basin. Moreover, late Carboniferous Sagsai gabbro–monzonite pluton intruding the Tugrug Group west of the studied area has a within-plate geochemical signature (Buriánek et al. 2016). Small bodies and dykes of early Permian fractionated granite are common in the central and eastern parts of the Bodonch–Tseel Zone (Kröner et al. 2010; Burenjargal et al. 2016; Hong et al. 2020) and the Devonian migmatised crust probably represents their source (Sukhbaatar et al. 2022).

2.4. Geological context of the studied samples

The studied rocks are exposed in the left tributary of the Gegeetiin Gol in the Ar Dalangiin Range (Fig. 1c), about 50 km south of Biger soum in the Gobi Altai province. Weakly metamorphosed volcano-sedimentary rocks originally attributed to Ukhinuur Formation (Rauzer et al. 1987) are recently interpreted as the upper part of the Cambrian–Ordovician Tugrug Group (Jiang et al. 2017; Hanžl et al. 2020). These rocks are exposed between the Lower Devonian terrigenous clastic sediments with the reef limestones of the Gichigeny Formation in the north and metamorphic rocks of the Bodonch–Tseel Zone in the south.

Dark grey turbidite deposits with an alternation of metasandstones, metasiltstones and phyllites occur along

the northern margin of the Bodonch–Tseel Zone. They show a maximum depositional age of *c.* 458 Ma according to the clastic zircons (Kröner et al. 2010), thereby indicating late Ordovician–Silurian age of the turbidite sequence (Fig. 1c). Further west, these rocks were intruded by the late Devonian granite (Hanžl et al. 2016).

The dominant lithologies of the Tugrug Group in the studied area are chlorite-sericite schists alternating with greenschists, phyllites and metasandstones. The bedding is parallel to NW–SE trending foliation steeply to moderately dipping to the SW or NE. The granitic body (17×2 km) is exposed in the southern part of the section and is elongated parallel with the strike of the foliation in the host rocks. Its northeastern contact is modified by fault, while the southwestern one is intrusive, irregular, and overprinted by metamorphic fabric. Both granite and its host rocks were affected by the greenschist–facies metamorphism, which was, based on analogy with adjacent areas, probably of Devonian age.

Sample **P605** (E 97.191933°; N 45.218369°) represents mylonitic metarhyolite (Fig. 2a) with quartz phenocrysts (up to 5 mm in size) forming a few meters thick layer in dark grey tuffitic metasiltstone. Asymmetric pressure shadows are developed around the rounded quartz porphyroclasts, which are locally recrystallised along their margins. Scarce angular grains of K-feldspar (1–2 mm across) are sericitised. Rare lithic fragments are flattened. The ultra-fine-grained groundmass is composed of quartz, sericite and chlorite, preferably oriented parallel to the foliation. Titanite and zircon are common accessory minerals. Tiny quartz veins are parallel with foliation as well as limonite bands. Carbonatisation of matrix is locally visible.

Sample **D574** (E 97.185593°; N 45.212433°) is medium- to coarse-grained biotite metagranite with cataclastic texture (Fig. 2b). Subangular quartz, K-feldspar and plagioclase grains up to 5 mm in size are irregularly fragmented and fractured. Anastomose network of shear planes is filled by a fine-grained groundmass composed of recrystallised quartz, chlorite, sericite, and carbonate. Biotite forms rare, partly chloritised aggregates. Accessory minerals are represented by opaque minerals, zircon, apatite, and monazite.

3. Methodology

3.1. Laser-ablation ICP-MS U–Pb dating of zircon

Zircon grains were separated using conventional techniques (crushing, grinding, sieving, Wilfley gravity separation table, magnetic and heavy-liquid separation) at the Central Geological Laboratory in Ulaanbaatar.

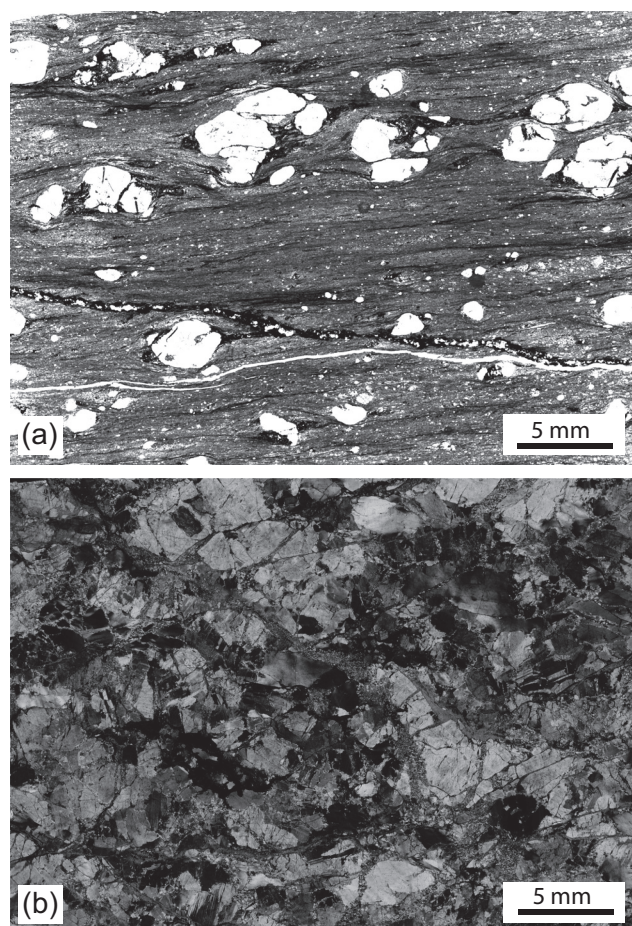


Fig. 2 Photomicrographs illustrating textures of studied rocks: **a** – Mylonitic metarhyolite P605 with quartz porphyroclasts surrounded by ultra-fine-grained matrix consisting of sericite, chlorite and micron-sized fragments of quartz and feldspars. Plane polarized light. **b** – Mylonitic metagranite D574 with fractured feldspars grains of various size. Fractured quartz grains are characterised by undulatory extinction, deformation bands and minor cataclasis along grain boundaries. Both quartz and feldspar fragments are surrounded by chloritised flakes of biotite and fine-grained bands composed of sericite and chlorite with an admixture of opaque minerals. Cross polarized light.

Subsequently, individual zircons were hand-picked from the zircon concentrate using a binocular microscope, embedded in epoxy resin and polished. Zircon internal structure and zoning were imaged using cathodoluminescence (CL) and back-scattered electrons (BSE) detectors mounted on a scanning electron microscope at the Joint Laboratory of the Masaryk University and the Czech Geological Survey in Brno.

The U–Th–Pb isotopic ratios in zircons were measured by an Analyte Excite 193 nm excimer laser-ablation system (LA, Photon Machines) equipped with a two-volume HelEx ablation cell in tandem with an Agilent 7900x ICP-MS housed at the Czech Geological Survey. The ablation took place in a He atmosphere ($0.8 \text{ l} \times \text{min}^{-1}$), the laser frequency was 5 Hz, the laser fluence $7.59 \text{ J} \times \text{cm}^{-2}$ and the beam diameter 25 μm . Each measurement consisted

of 20 s integration of the entrainment background signal and another 40 s integration of the sample ablation signal for masses 202, 204, 206, 207, 208, 232 and 238 using a SEM detector with one point per mass peak and mass integration times 10, 10, 15, 30, 20, 10 and 15 ms (total cycle time 0.134 s). To maintain stability of the instrument and ensure the reliability of the measured results, international zircon standard 91500 as the primary reference material and Plešovice (mean ID-TIMS U–Pb age of $337.13 \pm 0.37 \text{ Ma}$ (2σ) – Sláma et al. 2008) and GJ-1 (TIMS $^{207}\text{Pb}/^{206}\text{Pb}$ age of $608.5 \pm 0.4 \text{ Ma}$; Jackson et al. 2004) zircons as the secondary reference materials were measured after every ten sample points. Instrumental drift throughout the measurement was monitored by repeated analyses of the reference zircon 91500 (TIMS $^{207}\text{Pb}/^{206}\text{Pb}$ age $1065.4 \pm 0.3 \text{ Ma}$; Wiedenbeck et al. 1995).

Data processing was performed using Iolite software as described in Paton et al. (2011), including background correction, followed by laser-induced elemental fractionation (LIEF) correction based on comparison with the behaviour of the reference zircon 91500 with concordant age of $1063 \pm 2 \text{ Ma}$ for both samples (D574, P605). During this study, two reference materials were periodically analysed, giving concordant ages of $338 \pm 1 \text{ Ma}$ for both samples (Plešovice zircon) or $608 \pm 2 \text{ Ma}$ (GJ-1 in the case of sample D574) and $610 \pm 1 \text{ Ma}$ (GJ-1 in case of sample P605).

The data obtained (ESM 1) were statistically adjusted, including propagation of the relative error on the primary reference material, according to Horstwood et al. (2016). The propagated uncertainties were used to plot the mean and concordia ages using the IsoplotR software (Vermeesch 2018). The Wetherill plots are presented for individual samples. No common Pb correction was employed.

3.2. Whole-rock geochemistry

Major and trace elements in fresh whole-rock samples (3–4 kg) were determined in the Bureau Veritas Minerals (Vancouver) by ICP-OES/MS. The dissolution of the samples was by $\text{LiBO}_2/\text{Li}_2\text{B}_4\text{O}_7$ fusion in order to determine precisely also trace elements stored in refractory accessory phases. Detection limits were 0.01 % and better for major elements, 2 ppm and better for trace elements used for our geochemical interpretation and 0.05 ppm and better for REE.

Data management, recalculation, plotting and statistical evaluation of the whole-rock geochemical data were facilitated by *GCDkit* (Janoušek et al. 2006). In this work, the A/CNK index, uncorrected for apatite (Shand 1943), is defined as $\frac{\text{Al}_2\text{O}_3}{\text{CaO} + \text{Na}_2\text{O} + \text{K}_2\text{O}}$ [mol.%]. For a description of chondrite-normalized REE patterns serves the Eu/Eu^* ratio, reflecting the magnitude of the Eu anomaly ($\frac{\text{Eu}}{\text{Eu}^*} = \frac{\text{Eu}_N}{\sqrt{\text{Sm}_N \text{Gd}_N}}$), where N refers to concentrations normal-

ized to chondritic abundances (Boynnton 1984). Our data were plotted together with available data (see sources in the caption of Fig. 4) from the late Ordovician to early Silurian felsic magmatic rocks from the Mongolian Altai Domain to reveal possible correlations.

4. Results

4.1. Zircon U–Pb dating

Overall, 99 spots were measured on 83 grains in the metarhyolite sample **P605**, 76 spots of 65 grains were subsequently used for age calculation (ESM 1). Most of the grains are euhedral, bipyramidal, transparent or light brown to yellowish brown, with aspect ratio 1 : 2 to 1 : 3 in the more common stubby short prismatic grains with the length of 50–200 μm (Fig. 3a). The smallest grains are, in a few cases, partly corroded, acquiring a suboval irregular shape (grains No. Z69, Z73; Fig. 3a). Long-prismatic grains with the length of *c.* 300 μm and an aspect ratio of 1 : 5 to 1 : 6 are less frequent. However, the internal texture seems not to correlate with the shape of the individual grains. Generally, a well-developed brightly luminescent core surrounded by an oscillatory zoned rim is characteristic of the majority of the grains. Two or three relatively thick (*c.* 5–10 μm) external growth zones are common, fine multiple oscillatory zoning is not exceptional. Occasionally, a hint of lamellar texture (Z6) or sector zoning “overprint” (Z37) can be observed. Apart from this general texture, further processes are evident from the grains. Blurred (Z57), ghost (Z15) and convolute zoning (Z60) as features typical of solid-state recrystallisation (Hoskin and Black 2000) are seen in some grains. A few of them (Z7, Z8) suffered magmatic dissolution. Corroded internal zones in grains Z3, Z14, Z51 (Fig. 3a) likely point to a later metamictisation. The U concentrations are 53–281 ppm, Th/U ratios 0.1–0.6. The calculated concordia age of 457 ± 2 Ma (Fig. 3b) represents the magmatic formation age. The individual ages yield a fairly wide variance (*c.* 480 to 440 Ma, ESM 1) suggesting, together with zircon CL characteristics, alteration, and lead loss related to the late-stage magmatic processes.

In the metagranite sample **D574** 179 spots were measured on 96 zircon grains; 129 spots of 79 grains were used for age calculation. The zircon grains are euhedral, bipyramidal, transparent, or honey-brown in colour, 100–200 μm long with an aspect ratio 1 : 2 to 1 : 3 (Fig. 3c). Long-prismatic grains (*c.* 200 μm , aspect ratio 1 : 5) are exceptional (grains No. 47, 58; Fig. 3c). The original magmatic texture with the core overgrown by numerous thin oscillatory zones is widespread. Grains with partially

resorbed cores overgrown subsequently by regular zones are not unique (20, 68). In cases, it is possible to observe the replacement of the oscillatory zoning by sector zoning (15, 66). Sometimes also effects of different degrees of recrystallisation, or even resorption of the grain, are seen (76). Several grains had to be excluded from dating because of their complete alteration (86, 93). The U concentrations vary between 34 and 1300 ppm (ESM 1), Th/U ratios range 0.08–2.4, with an exceptional value of 25.5 in the grain 4 that was excluded from the dating. The determined concordia age 445 ± 1 Ma (Fig. 3d) dates the pluton emplacement.

4.2. Whole-rock geochemistry

The studied rocks are SiO_2 -rich (75 wt. % for granite and 70 wt. % for metarhyolite, Tab. 1). Sample D574 is classified as granite and sample P605 as rhyolite to

Tab. 1 Major- and trace-element whole-rock geochemical data from the studied samples

(wt. %)	D574	P605	(ppm)	D574	P605
SiO_2	75.08	70.25	Sb	1	1.2
TiO_2	0.23	0.54	Cs	3.6	5.3
Al_2O_3	12.99	13.48	Ba	490	816
Fe_2O_3	1.67	4.38	Nb	9.0	12.1
MnO	0.03	0.13	Ta	1.03	1.12
MgO	0.40	1.22	W	3.2	3.9
CaO	0.57	1.29	Tl	0.74	0.59
Na_2O	3.50	1.17	Pb	16	8
K_2O	4.52	3.72	Bi	<0.1	0.1
P_2O_5	0.07	0.23	Th	10.8	17
LOI	0.70	2.71	U	3.30	2.15
Total	99.76	99.14	La	19.6	45.4
			Ce	45.0	99.6
(ppm)	D574	P605	Pr	5.21	11.60
Be	2	2	Nd	20.4	45.3
Sc	5	9	Sm	4.95	10.10
V	14	47	Eu	0.689	1.650
Cr	10	30	Gd	4.83	9.27
Co	2	5	Tb	0.98	1.49
Ni	10	10	Dy	6.56	8.80
Cu	5	5	Ho	1.32	1.78
Zn	15	40	Er	4.16	4.82
Ga	13	16	Tm	0.606	0.683
Ge	1.6	1.8	Yb	3.80	4.52
As	<5	10	Lu	0.569	0.704
Rb	138	133			
Sr	75	57	FeOt	1.50	3.94
Y	38.2	46.4	$\text{K}_2\text{O}/\text{Na}_2\text{O}$	1.29	3.18
Zr	104	243	A/NK	1.22	2.26
Hf	3.1	5.7	A/CNK	1.11	1.62
Mo	<1	<1	ΣREE	118.7	245.7
Ag	<0.5	0.8	Eu/Eu*	0.43	0.52
In	<0.1	<0.1	La_N/Yb_N	3.48	6.77
Sn	3	4	Gd_N/Lu_N	1.06	1.64

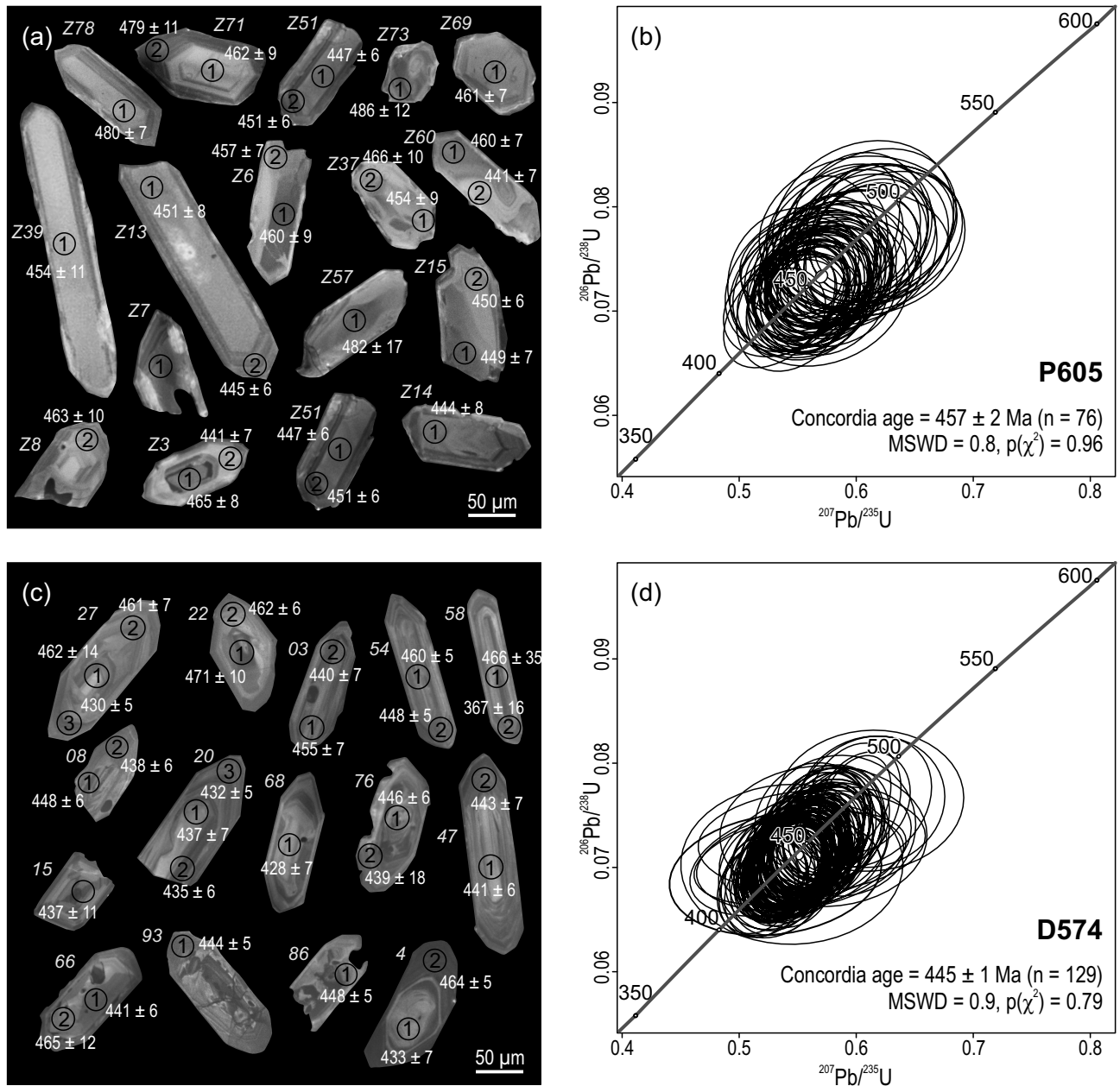


Fig. 3 Cathodoluminescence images of representative zircon grains with analytical spots labelled by individual $^{206}\text{Pb}/^{238}\text{U}$ ages ($\pm 2\sigma$ Ma) and U-Pb Wetherill concordia plots for the studied samples: **a, b** – metarhyolite P605; **c, d** – metagranite D574.

rhyodacite based on the TAS (total alkali–silica) and Zr/TiO₂–SiO₂ classification diagrams (Figs 4a, b; Cox et al. 1979 and Winchester and Floyd 1977, respectively). Both of the samples are peraluminous (A/CNK = 1.1 for granite and 1.6 for metarhyolite) and high-K calc-alkaline (K₂O/Na₂O = 1.3 and 3.2) based on SiO₂ vs. K₂O (Peccerillo and Taylor 1976; not shown) or Co vs. Th diagrams (Fig. 4c; Hastie et al. 2007).

Chondrite-normalised (Boynton 1984) REE patterns of both the studied samples display similar trends (Fig. 5a, b) characterised by enrichment of LREE (La_N/Yb_N = 3.5 and 6.8), pronounced negative Eu anomalies

(Eu/Eu* = 0.43 for granite and 0.52 for rhyolite) and relatively flat trend towards HREE (Gd_N/Lu_N = 1.06 and 1.64). However, total REE contents in the granite (119 ppm) are two times lower than in the rhyolite (246 ppm).

Also, normal Mid-Ocean Ridge Basalt (NMORB) normalised (Sun and McDonough 1989) spider plots (Fig. 5c, d) show nearly identical patterns for granite and rhyolite with strong enrichments in Large Ion Lithophile Elements (LILE) (Cs, Rb, Ba and K) as well as in Th, U and Pb. Negative anomalies in Nb, Sr, P and Ti are pronounced.

5. Discussion

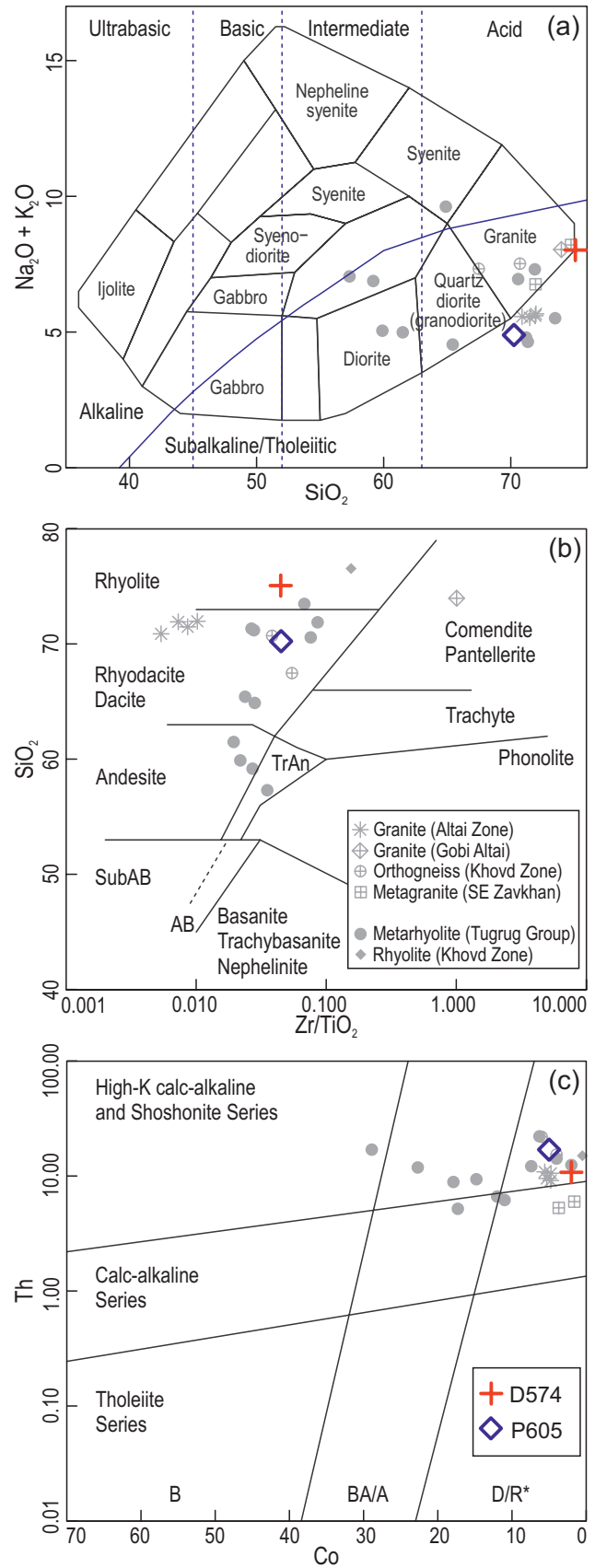
5.1. Age and regional correlations of Ordovician magmatic rock in the Mongolian Altai Domain and adjacent areas

Palaeozoic evolution of the Mongolian Altai Domain was characterised by a late Ordovician–Silurian gap within a mainly basaltic igneous activity (Buriánek et al. 2022; Hanžl et al. 2023). The late Ordovician is considered to have witnessed the end of growth of volcano-sedimentary system above the retreating subduction zone (Jiang et al. 2017; Buriánek et al. 2022) followed by crustal thickening and metamorphism (Soejono et al. 2021). Indeed, products of late Ordovician magmatic activity are scarce and only randomly distributed in the MAW and adjacent units (Fig. 1b). The main question that arose from the presented data is in possible correlation of the studied late Ordovician plutonic and volcanic rocks with coeval magmatic activity reported by other authors. The second goal is to interpret the new data in the frame of a recent geodynamic model of the Mongolian Altai Domain.

5.1.1. Volcanic rocks

Metabasalts and metarhyolites are common members of the Cambrian–Ordovician Tugrug Group in the Gobi Altai (Kröner et al. 2010; Hanžl et al. 2019). Volcano-clastic rocks of this group are generally older (511–465 Ma, Jiang et al. 2017) than rhyolite sample P605 (457 ± 2 Ma) reported in this study. These rocks show high compositional variability, which could be caused by irregular clastic admixture (Jiang et al. 2017). Nevertheless, geochemical signatures of some of them could be correlated with the sample P605 (Figs 4–5). Nearly identical geochemical signature and age yielded rhyolitic ignimbrite from the Botgoniigol Formation in the westerly Khovd Zone (462 ± 3 Ma, Buriánek et al. 2022).

Fig. 4 Whole-rock geochemical classification of studied rocks and comparison with late Ordovician magmatic rocks from the Mongolian Altai Domain and adjacent areas. **a** – Total alkali–silica (TAS) diagram according Cox et al. (1979) with the alkaline/subalkaline boundary of Irvine and Baragar (1971). **b** – Zr/TiO₂ versus SiO₂ classification diagram of Winchester and Floyd (1977). **c** – Binary plot Co–Th (Hastie et al. 2007) designed to distinguish between various suites of altered subalkaline volcanic rocks. Source data: granite (Altai Zone) – Zhang et al. (2017b); granite (Gobi Altai) – Helo et al. (2006); orthogneiss (Khovd Zone) – Soejono et al. (2017); metagranite (SE Zavkhan) – Kozakov et al. (2012); metarhyolite (Tugrug Group) – Jiang et al. (2017); rhyolite (Khovd Zone) – Buriánek et al. (2022). Explanations: TrAn – trachyandesite, SubAB – subalkaline basalt, AB – alkaline basalt, B – basalt, BA/A – basaltic andesite and andesite, D/R* – dacite and rhyolite.



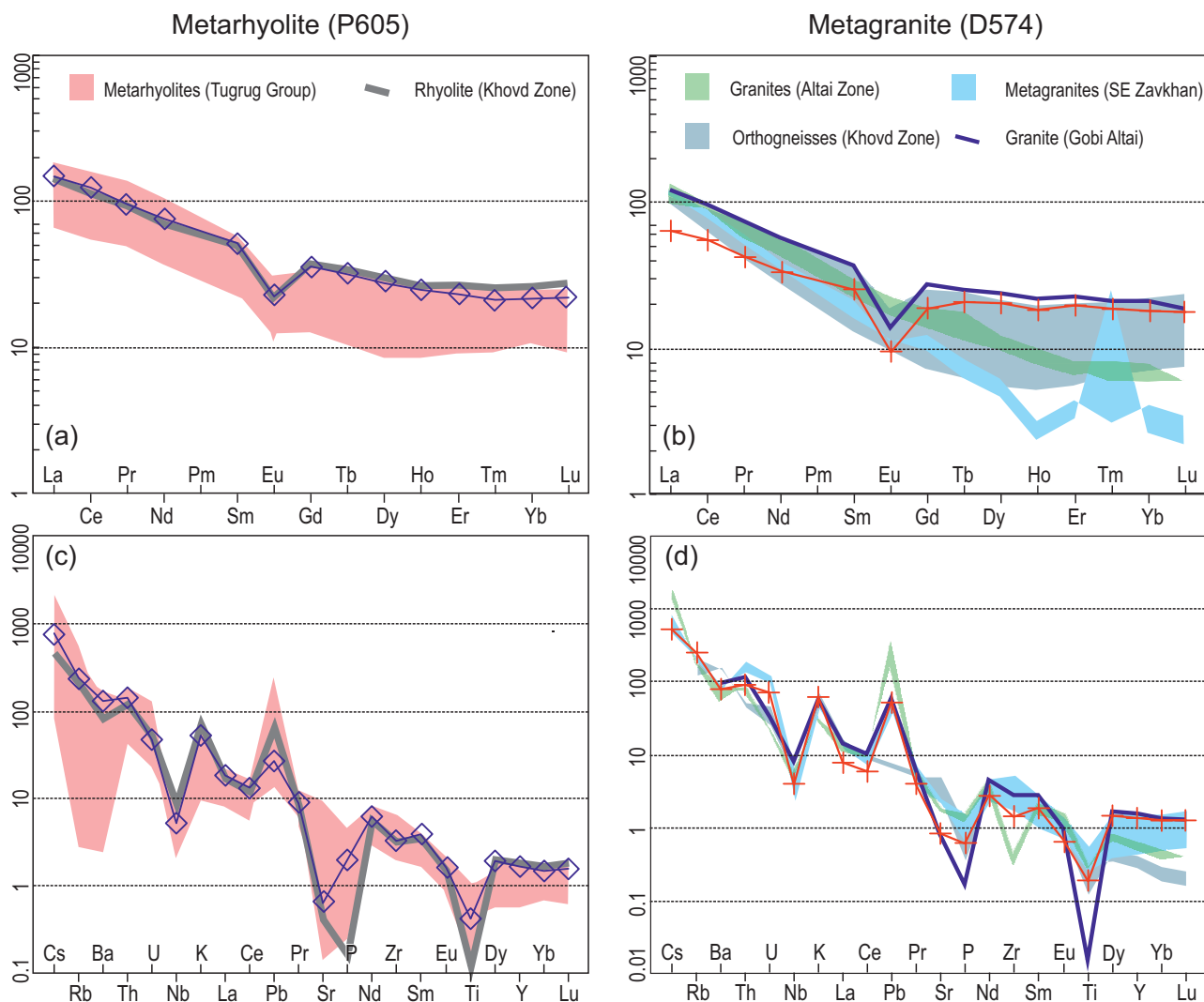


Fig. 5 Spider diagrams for studied rocks and their comparison with late Ordovician magmatic rocks in Mongolian Altai. Data sources as in Fig. 4. Chondrite-normalised (Boynnton 1984) REE patterns for metarhyolite P605 (a) and metagranite D574 (b). Normal Mid-Ocean Ridge Basalt (NMORB)-normalised trace-element patterns (Sun and McDonough 1989) for metarhyolite P605 (c) and metagranite D574 (d).

Felsic pyroclastic rocks in easterly Lower Palaeozoic volcano-sedimentary sequences on the S slopes of the Arz Bogd Mountain were dated to 441 ± 8 Ma and metadacite south of Bayanlig to 443 ± 5 Ma (Kröner et al. (2017). Zircon Hf isotopic data of these volcanic rocks indicate mixed crustal source of the Neoproterozoic to Mesoproterozoic age. Middle to late Ordovician bimodal volcanism (476–446 Ma) was reported from the northern part of Altai–Sayan area (north-western continuation of the Mongolian Altai Domain) and interpreted as a product of interaction of magmas generated from a mantle source with crustal rocks in the intracontinental geotectonic regime (Vorontsov et al. 2019).

5.1.2. Plutonic rocks

Biotite metagranite D574 representing the local intrusive body in the Tugrug Group yields the age of 445 ± 1

Ma fitting the Ordovician–Silurian boundary. Nearly no plutonic rocks of a similar age are known from the Mongolian Altai Domain.

This age correlates well with the local zircon population minimum *c.* 449–446 Ma in the Chinese Altai represented by muscovite–biotite granites with sillimanite (Zhang et al. 2017a). These rocks interpreted as heterogeneous S-type granites differ from our sample in modal composition and whole-rock geochemistry including REE patterns (Fig. 5b). Syn-metamorphic gneissose granite dated at 448 ± 2 Ma was also reported from the southern margin of the Zavkhan Block (Kozakov et al. 2012) but shows geochemical composition unlike the studied metagranite sample D574 (Figs 4–5). In the Khovd Zone, early–mid Ordovician plutonic rocks (*c.* 476–460 Ma) of oceanic-arc geochemical signatures were related to the evolution of the Cam-

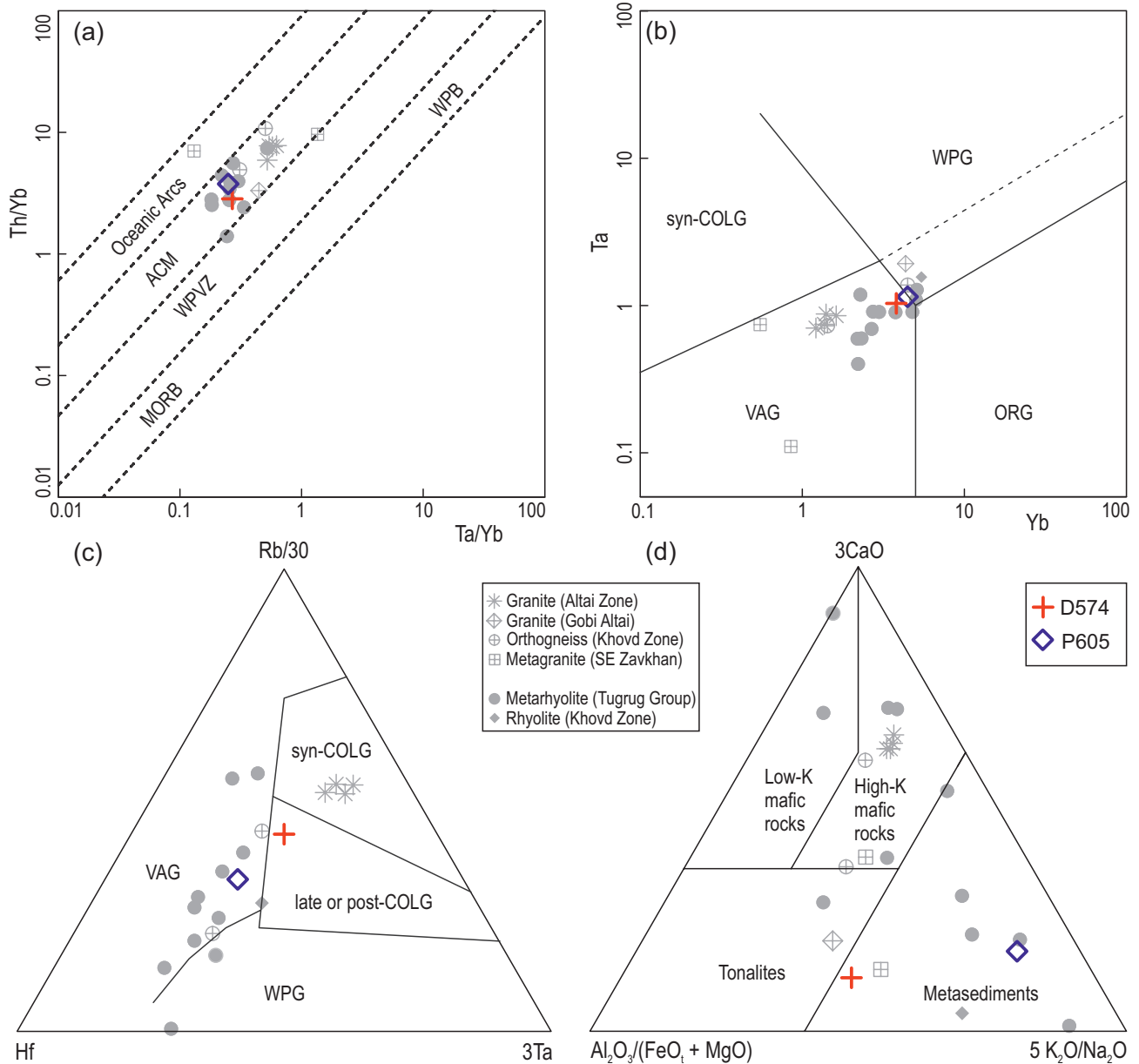


Fig. 6 Selected geotectonic diagrams. **a** – Ta/Yb vs. Th/Yb binary plot of Schandl and Gorton (2002). **b** – Geotectonic diagram Yb–Ta (ppm) of Pearce et al. (1984). **c** – Triangular plot Hf–Rb/30–3 Ta (Harris et al. 1986) for classification of collision-related granites. **d** – Ternary plot $Al_2O_3/(FeO_t + MgO) - 3 \times CaO - 5 \times K_2O/Na_2O$ (wt. %) of Laurent et al. (2014) to distinguish likely sources of granitic melts. Explanations: ACM – Active Continental Margin, WPVZ – Within-Plate Volcanic Zone, WPB – Within-Plate Basalts, MORB – Mid-Oceanic Ridge Basalts, VAG – Volcanic-Arc Granites, ORG – Ocean Ridge Granites, WPG – Within-Plate Granites, syn-COLG – syn-collision peraluminous leucogranites, late or post-COLG – late or post-collision calc-alkaline intrusions. Data sources as in Fig. 4.

brian–Ordovician Ikh-Mongol Arc System (Soejono et al. 2016; Buriánek et al. 2022). Late Silurian metagranite (425.5 ± 1.1 Ma; Helo et al. 2006) from the eastern Gobi Altai Zone, geochemically similar to the studied granite (Figs 4–5) was interpreted as having developed in transitional magmatic arc recycling crustal materials. Finally, Kröner et al. (2017) described undeformed porphyritic arc granite yielding a middle Ordovician age of 467 ± 3 Ma from the same area.

5.2. Geotectonic constraints on the late Ordovician magmatism in the Mongolian Altai Domain

5.2.1. Whole-rock geochemical constraints on geotectonic setting

Based on the whole-rock geochemistry, the studied rhyolite sample can be generally correlated with some

metarhyolites from the Tugrug Group. However, the metagranite differs from the Ordovician granitoids of the Mongolian Altai Domain and adjacent areas, mainly in the REE patterns (Fig. 5).

In the diagram Ta/Nb vs. Th/Yb (Schandl and Gorton 2002) our samples, together with the other Ordovician granites and rhyolites from the area, show signatures typical of magmatic rocks of the active continental margins (Fig. 6a). In the diagram Yb vs. Ta (Pearce et al. 1984) they straddle the boundary between volcanic-arc and within-plate granites (Fig. 6b), which is typical of post-collisional granites (Pearce 1996). Positions of samples in ternary diagram Hf–Rb/30–3 × Ta (Harris et al. 1986) correspond well with the age and field relationships of studied rocks. While the older rhyolite is a part of the Tugrug volcano-sedimentary sequence and fits the volcanic arc field, the younger granite intruded the sequence and plots in the field of late- or post-collisional granite just close the boundary with the volcanic-arc granite (Fig. 6c).

Both samples show nearly identical NMORB-normalised trends (Fig. 5c–d) characterised by arc-like enrichment of LILE (mobile in hydrous fluids) over geochemically conservative HFSE (high field strength elements) contributed solely by the mantle wedge (Saunders et al. 1991; Pearce and Peate 1995; Tatsumi and Eggins 1995; Pearce et al. 2005) and could point to a similar magma source and petrogenesis. High-K calc-alkaline and peraluminous character of the studied rocks corresponds with position in the field representing the melting of metasediments in the ternary discrimination diagram $Al_2O_3/(FeO+MgO)-3 \times CaO-5 \times K_2O/Na_2O$ of Laurent et al. (2014).

There were found no obvious inherited zircons but the ages of *c.* 460 Ma detected in several zircon cores in both samples could also indicate a similar magma source possibly represented by immature sediments typical of the MAW. Altogether, the source of the studied rhyolite and granite was likely dominated by detritus derived from the Cambrian–early Ordovician magmatic rocks of the Ikh-Mongol Arc System located further north.

5.2.2. Geotectonic setting of the late Ordovician magmatism

Clastic sediments of the Cambrian–Ordovician Tugrug Fm. were interpreted to be of passive continental margin affinity (Zonenshain 1973). On the contrary, Mossakovsky and Dergunov (1985) considered deposition of this sequence in arc-related tectonic setting. Relatively high contents of MgO and Cr compared to typical passive continental margin sediments and immature turbidite-like sediments of the Tugrug Group indicate a deposition in a fore-arc basin of the Ikh-Mongol Arc System, with a dominant source in felsic to intermediate rocks of

volcanic origin (Jiang et al. 2017; Buriánek et al. 2022; Sukhbaatar et al. 2022).

On the other hand, deposition of protolith to similar low-grade metasedimentary rocks in NW Mongolian Altai was not older than early Silurian according to clastic zircon spectra (Long et al. 2019). Maximum depositional age of protoliths to the metamorphic rocks of the Bodonch–Tseel Zone is supposed to be older – Cambrian–Ordovician and late Ordovician–early Silurian (Sukhbaatar et al. 2022). The section of the Tugrug Group in Ar Dalangiin Range area is not younger than late Ordovician as indicated by radiometric age of sample D574 representing a granitic pluton intruding the entire sequence.

The compositional variability of late Ordovician granitoids and felsic volcanic rocks in the MAW indicates that using geochemical tectonic discrimination diagrams could be misleading, and more probably reflects the variability of the sedimentary and volcano-sedimentary sources themselves derived from the Cambrian–Ordovician arc and the Precambrian basement to the north (e.g., Jiang et al. 2016; Huang et al. 2020). Comparable observation was made for another early Palaeozoic accretionary system, the Lachlan Orogen in SE Australia (Collins et al. 2020).

Similar geochemistry of studied metarhyolite and metagranite and the narrow time gap between their intrusive ages allows placing their emplacement to the final stage of the Mongolian Altai accretionary wedge development. This episode was younger than the youngest parts of the Cambrian–Middle Ordovician Ikh-Mongol Arc System set to 460 Ma in Khovd Zone (Soejono et al. 2016) and to 485 Ma in the Zamtyn Nuruu Range of the Lake Zone (Hrdličková et al. 2010) but it was close to the deposition of immature greywackes in the Bodonch–Tseel Zone (Sukhbaatar et al. 2022).

Recently, Soejono et al. (2021) proposed that the late Ordovician was a period associated to the earliest stage of the Barrovian metamorphism and thickening of the MAW. The thickening of the wedge was characterised by a volcanic gap in late Ordovician–early Silurian sequences (Buriánek et al. 2022). Therefore, in agreement with a model of Collins et al. (2020), the onset of late Ordovician magmatism may indicate onset of post-contraction magmatism related to melting of diverse volcano-sedimentary packages within the MAW.

Alternatively, the rare early Palaeozoic magmatism may indicate that the MAW formed in a fore-arc basin (see also Sukhbaatar et al. 2022), whose melting might be related to late stages of Ikh-Mongol Arc System migration controlled by southward roll-back of the oceanic plate (Soejono et al. 2017; Janoušek et al. 2018). Taken together, the scarce late Ordovician magmatic activity in the Gobi Altai Zone recorded a missing segment in

tectono-thermal history of the Mongolian Collage, which deserves further investigations.

6. Conclusions

- Late Ordovician metarhyolite (457 ± 2 Ma) found in the Ar Dalangiin range (Gobi Altai Zone of Mongol Altai Domain) is interpreted as a product of the subaerial volcanism in the uppermost member of the Cambrian–Ordovician Tugrug Group.
- The nearby late Ordovician intrusive body of biotite granite (445 ± 1 Ma) likely post-dated maximum sedimentation age of the Tugrug Group.
- Metarhyolite and metagranite bear geochemical signatures of igneous rocks of an active continental margin and their whole-rock geochemistry shows common parental magma sources. They were likely derived by partial melting of Cambrian to early Ordovician lithologies at late- to post-tectonic stages of the Mongolian Altai accretionary wedge evolution.
- Late Ordovician magmatic rocks of various geochemical compositions, very rare in the Mongolian Altai Domain, could represent sporadic magmatic activity related to post-contraction event connected with shortening and thickening of the Cambrian–Ordovician fore-arc basin. It was followed by the initiation of the Silurian–Devonian back-arc basin opening.

Acknowledgments. The research was realized in the frame of the project GAČR EXPRO 19-27682X. The manuscript was improved much thanks to detailed reviews of two anonymous reviewers, and further benefited from the careful editorial work of handling editor V. Janoušek. We thank A. Zavřelová for preparation of zircon CL images.

Electronic supplementary material. Laser-ablation ICP-MS U–Pb data from dated zircons are available at the Journal web site (<http://dx.doi.org/10.3190/jgeosci.385>).

References

- BADARCH G, CUNNINGHAM WD, WINDLEY BF (2002) A new terrane subdivision for Mongolia: implications for the Phanerozoic crustal growth of Central Asia. *J Asian Earth Sci* 21: 87–104
- BIBIKOVA VE, KIRNOZOVA TI, KOZAKOV IK, KOTOV AB, NEYMARK LA, GOROKHOVSKIY BM, SHULESHKO IK (1992) U–Pb ages for polymetamorphic complexes on the southern flank of the Mongolian and Gobi Altai. *Geotectonics* 26: 166–172
- BOLD U, CROWLEY JL, SMITH EF, SAMBUU O, MACDONALD FA (2016) Neoproterozoic to early Paleozoic tectonic evolution of the Zavkhan Terrane of Mongolia: implications for continental growth in the Central Asian Orogenic Belt. *Lithosphere* 8: 729–750
- BOLDBAATAR D, OSANAI Y, NAKANO N, ADACHI T, SEREENEN J, KITABO I, SYERRYEKHAN K (2021) Geochronology and geochemistry of granitoids from the Mongolian Altai. *J Mineral Petrol Sci* 116: 293–308
- BORZAKOVSKII YA (1985) Compilation of geological map and map of the ore deposits of the Western Mongolia (west of meridian 102°) at a scale of 1 : 500,000 with explanation text, 1st stage, compilation of map sheets M-46B, G; L-47A, B, V, G. Zarubezgeologiya, Moscow (in Russian)
- BOYNTON WV (1984) Cosmochemistry of the rare earth elements: meteorite studies. In: HENDERSON P (ed) *Rare Earth Element Geochemistry*. Elsevier, Amsterdam, pp 63–114
- BROUSSOLLE A, ŠTÍPSKÁ P, LEHMANN J, SCHULMANN K, HACKER BR, HOLDER R, KYLANDER-CLARK ARC, HANŽL P, RACEK M, HASALOVÁ P, LEXA O, HRDLIČKOVÁ K, BURIÁNEK D (2015) P–T–t–D record of crustal-scale horizontal flow and magma-assisted doming in the SW Mongolian Altai. *J Metamorph Geol* 33: 359–383
- BROUSSOLLE A, SUN M, SCHULMANN K, GUY A, AGUILAR C, ŠTÍPSKÁ P, JIANG YD, YU Y, XIAO WJ (2019) Are the Chinese Altai “terrane” the result of juxtaposition of different crustal levels during Late Devonian and Permian orogenesis? *Gondwana Res* 66: 183–206
- BURENJARGAL U, OKAMOTO A, KUWATANI T, SAKATA S, HIRATA T, TSUCHIYA N (2014) Thermal evolution of the Tsel Terrane, SW Mongolia and its relation to granitoid intrusions in the Central Asian Orogenic Belt. *J Metamorph Geol* 32: 765–790
- BURENJARGAL U, OKAMOTO A, TSUCHIYA N, UNO M, HORIE K, HOKADA T (2016) Contrasting geochemical signatures of Devonian and Permian granitoids from the Tsel Terrane, SW Mongolia. *J Geosci* 61: 51–66
- BURIÁNEK D, JANOUŠEK V, HANŽL P, JIANG YD, SCHULMANN K, LEXA O, ALTANBAATAR B (2016) Petrogenesis of the Late Carboniferous Sagsai Pluton in the SE Mongolian Altai. *J Geosci* 61: 67–92
- BURIÁNEK D, SCHULMANN K, HRDLIČKOVÁ K, HANŽL P, JANOUŠEK V, GERDES A, LEXA O (2017) Geochemical and geochronological constraints on distinct Early-Neoproterozoic and Cambrian accretionary events along southern margin of the Baydrag Continent in western Mongolia. *Gondwana Res* 47: 200–227
- BURIÁNEK D, SOEJONO I, SCHULMANN K, JANOUŠEK V, HANŽL P, ČÁP P, BOLD U, SVOJTKA M, COLLETT S, ŽÁČEK V (2022) Subduction-controlled temporal and spatial variations in early Palaeozoic sedimentary and volcanic record of the Mongol-Altai Domain. *J Asian Earth Sci* 230: 105182

- CAI K, SUN M, YUAN C, LONG XP, XIAO WJ (2011) Geological framework and Paleozoic tectonic history of the Chinese Altai, NW China: a review. *Russ Geol Geophys* 52: 1619–1633
- CAI K, SUN M, JAHN BM, XIAO WJ, YUAN C, LONG XP, CHEN HY, TUMURKHUU D (2015) A synthesis of zircon U–Pb ages and Hf isotopic compositions of granitoids from southwest Mongolia: implications for crustal nature and tectonic evolution of the Altai Superterrane. *Lithos* 232: 131–142
- COCKS LRM, TORSVIK TH (2007) Siberia, the wandering northern terrane, and its changing geography through the Palaeozoic. *Earth Sci Rev* 82: 29–74
- COLLINS WJ, HUANG H Q., BOWDEN P., KEMP A I S. (2020) Repeated S–I–A-type granite trilogy in the Lachlan Orogen and geochemical contrasts with A-type granites in Nigeria: implications for petrogenesis and tectonic discrimination. In: JANOUŠEK V, BONIN B, COLLINS WJ, FARINA F, BOWDEN P (eds) *Post-Archean Granitic Rocks: Contrasting Petrogenetic Processes and Tectonic Environments*. Geological Society of London Special Publications 491, pp 53–76
- COX KG, BELL JD, PANKHURST RJ (1979) *The Interpretation of Igneous Rocks*. George Allen & Unwin, London, pp 1–450
- CUI X, SUN M, ZHAO GC, ZHANG YY (2021) Origin of Permian mafic intrusions in southern Chinese Altai, Central Asian Orogenic Belt: a post-collisional extension system triggered by slab break-off. *Lithos* 390–391: 106112
- CUNNINGHAM WD, DICKINSON WR (2006) Active intracontinental transpressional mountain building in the Mongolian Altai: defining a new class of orogen. *Earth Planet Sci Lett* 240: 436–444
- DASH B, BOLDBAATAR E, ZORIGTKHUU O-E, YIN A (2016) Geochronology, geochemistry and tectonic implications of Late Triassic granites in the Mongolian Altai Mountains. *J Asian Earth Sci* 117: 225–241
- DEMOUX A, KRÖNER A, HEGNER E, BADARCH G (2009) Devonian arc-related magmatism in the Tsel Terrane of SW Mongolia: chronological and geochemical evidence. *J Geol Soc London* 166: 459–471
- DIJKSTRA AH, BROUWER FM, CUNNINGHAM WD, BUCHAN C, BADARCH G, MASON PRD (2006) Late Neoproterozoic proto-arc ocean crust in the Dariv Range, western Mongolia: a supra-subduction zone end-member ophiolite. *J Geol Soc London* 163: 363–373
- HANŽL P, SCHULMANN K, JANOUŠEK V, LEXA O, HRDLIČKOVÁ K, JIANG YD, BURIÁNEK D, ALTANBAATAR B, GANCHULUUN T, ERBAN V (2016) Making continental crust: origin of Devonian orthogneisses from SE Mongolian Altai. *J Geosci* 61: 25–50
- HANŽL P, KREJČÍ Z, ALTANBAATAR B, LEXA O, BURIÁNEK D, JANOUŠEK V, SCHULMANN K, JIANG YD, HRDLIČKOVÁ K (2017) Geology of the Gobi Altai and Tsel terranes in the central part of the Sagsai River watershed, SE Mongolian Altai. *J Maps* 13: 270–275
- HANŽL P, LEXA O, SCHULMANN K (EDS) (2019) IGCP-662 Project ‘Orogenic Architecture and Crustal Growth from Accretion to Collision’ Field Guide, Chandman soum, Gobi-Altai Aimag. MUST, Ulaanbaatar
- HANŽL P, GUY A, BATTUSHIG A, LEXA O, SCHULMANN K, KUNCEOVÁ E, HRDLIČKOVÁ K, JANOUŠEK V, BURIÁNEK D, KREJČÍ Z, JIANG YD, OTGONBAATAR D (2020) Geology of the Gobi and Mongol Altai junction enhanced by gravity analysis: a key for understanding of the Mongolian Altaides. *J Maps* 16: 98–107
- HANŽL P, JANOUŠEK V, HRDLIČKOVÁ K, BURIÁNEK D, GEREL O, ALTANBAATAR B, HORA JM, ČOUPEK P (2023) From magmatic arc to a post-accretionary setting: Late Palaeozoic granitoid plutons in the northwestern Trans-Altai Zone, Mongolia. *J Geosci* 68: 25–66
- HARRIS NBW, PEARCE JA, TINDLE AG (1986) Geochemical characteristics of collision-zone magmatism. In: COWARD MP, RIES AC (eds) *Collisional Tectonics*. Geological Society of London Special Publications 19, pp 67–81
- HASTIE AR, KERR AC, PEARCE JA, MITCHELL SF (2007) Classification of altered volcanic island arc rocks using immobile trace elements: development of the Th–Co discrimination diagram. *J Petrol* 48: 2341–2357
- HELO C, HEGNER E, KRÖNER A, BADARCH G, TOMURTOGОО O, WINDLEY BF, DULSKI P (2006) Chemical signature of Paleozoic accretionary complexes of Central Asian Orogenic Belt in south Mongolia: constraints on arc environments and crustal growth. *Chem Geol* 227: 236–257
- HONG T, GAO J, XU XW, WU C, LI H (2020) Late Palaeozoic magmatism in the eastern Tsel Terrane of SW Mongolia evidenced by chronological and geochemical data. *Geol J* 56: 3415–3447
- HORSTWOOD MSA, KOŠLER J, GEHRELS G, JACKSON SE, MCLEAN NM, PATON C, PEARSON NJ, SIRCOMBE K, SYLVESTER P, VERMEESCH P, BOWRING JF, CONDON DJ, SCHOENE B (2016) Community-derived standards for LA-ICP-MS U–(Th–)Pb geochronology – uncertainty propagation, age interpretation and data reporting. *Geostand Geoanal Res* 40: 311–331
- HOSKIN PWO, BLACK LP (2000) Metamorphic zircon formation by solid-state recrystallization of protolith igneous zircon. *J Metamorph Geol* 18: 423–439
- HRDLIČKOVÁ K, GERDES A, GILÍKOVÁ H, BAT-ULZII D, HANŽL P (2010) Burd Gol granite massif as a product of the late Cambrian post-orogenic magmatism in the SE part of the Lake Zone, Gobi Altai, SW Mongolia. *J Geosci* 55: 369–386
- HUANG YQ, JIANG YD, COLLETT S, WANG S, XU K, SHU T, LI PF, YUAN C (2020) Magmatic recycling of accretionary wedge: a new perspective on Silurian–Devonian I-type

- granitoids generation in the Chinese Altai. *Gondwana Res* 78: 291–307
- IRVINE TN, BARAGAR WRA (1971) A guide to the chemical classification of the common volcanic rocks. *Canad J Earth Sci* 8: 523–548
- JACKSON SE, PEARSON NJ, GRIFFIN WL, BELOUSOVA EA (2004) The application of laser ablation-inductively coupled plasma-mass spectrometry to in situ U–Pb zircon geochronology. *Chem Geol* 211: 47–69
- JAHN BM, WU F, CHEN B (2000) Massive granitoid generation in Central Asia: Nd isotope evidence and implication for continental growth in the Phanerozoic. *Episodes* 23: 82–92
- JANOŠEK V, FARROW CM, ERBAN V (2006) Interpretation of whole-rock geochemical data in igneous geochemistry: introducing Geochemical Data Toolkit (GCDkit). *J Petrol* 47: 1255–1259
- JANOŠEK V, JIANG YD, BURIÁNEK D, SCHULMANN K, HANŽL P, SOEJONO I, KRÖNER A, ALTANBAATAR B, ERBAN V, LEXA O, GANCHULUUN T, KOŠLER J (2018) Cambrian–Ordovician magmatism of the Ikh-Mongol Arc System exemplified by the Khantaishir Magmatic Complex (Lake Zone, south–central Mongolia). *Gondwana Res* 54: 122–149
- JIAN P, KRÖNER A, JAHN BM, WINDLEY BF, SHI Y, ZHANG W, ZHANG F, MIAO L, TOMURHUU D, LIU D (2014) Zircon dating of Neoproterozoic and Cambrian ophiolites in west Mongolia and implications for the timing of orogenic processes in the central part of the Central Asian Orogenic Belt. *Earth Sci Rev* 133: 62–93
- JIANG YD, SUN M, ZHAO GC, YUAN C, XIAO WJ, XIA XP, LONG XP, WU FY (2011) Precambrian detrital zircons in the Early Paleozoic Chinese Altai: their provenance and implications for the crustal growth of Central Asia. *Precambrian Res* 189: 140–154
- JIANG YD, SUN M, KRÖNER A, TUMURKHUU D, LONG XP, ZHAO GC, YUAN C, XIAO WJ (2012) The high-grade Tsel Terrane in SW Mongolia: an Early Paleozoic arc system or a Precambrian sliver? *Lithos* 142–143: 95–115
- JIANG YD, SCHULMANN K, SUN M, ŠTÍPSKÁ P, GUY A, JANOŠEK V, LEXA O, YUAN C (2016) Anatectic accretionary wedge, Pacific-type magmatism, and formation of vertically stratified continental crust in the Altai Orogenic Belt. *Tectonics* 35: 3095–3118
- JIANG YD, SCHULMANN K, KRÖNER A, SUN M, LEXA O, JANOŠEK V, BURIÁNEK D, YUAN C, HANŽL P (2017) Neoproterozoic–Early Paleozoic Peri-Pacific accretionary evolution of the Mongolian Collage System: insights from geochemical and U–Pb zircon data from the Ordovician sedimentary wedge in the Mongolian Altai. *Tectonics* 36: 2305–2331
- KHAIN EV, BIBIKOVA EV, SAL'NIKOVA EB, KRÖNER A, GIB-SHER AS, DIDENKO AN, DEGTYAREV KE, FEDOTOVA AA (2003) The Palaeo-Asian Ocean in the Neoproterozoic and early Palaeozoic: new geochronologic data and palaeotectonic reconstructions. *Precambr Res* 122: 329–358
- KHUKHUDEI U, KUSKY T, WINDLEY BF, OTGONBAYAR O, WANG L (2022) Ophiolites and ocean plate stratigraphy (OPS) preserved across the Central Mongolian Microcontinent: a new mega-archive of data for the tectonic evolution of the Paleo-Asian Ocean. *Gondwana Res* 105: 51–83
- KOZAKOV IK, SAL'NIKOVA EB, YARMOLYUK VV, KOZLOVSKY AM, KOVACH VP, AZIMOV PY, ANISIMOVA I V, LEBEDEV VI, ENJIN G, ERDENEJARGAL C, PLOTKINA YV, FEDOSEENKO AM, YAKOVLEVA SZ (2012) Convergent boundaries and related igneous and metamorphic complexes in Caledonides of Central Asia. *Geotectonics* 46: 16–36
- KRÖNER A, LEHMANN J, SCHULMANN K, DEMOUX A, LEXA O, TOMURHUU D, ŠTÍPSKÁ P, LIU D, WINGATE MTD (2010) Lithostratigraphic and geochronological constraints on the evolution of the Central Asian Orogenic Belt in SW Mongolia: Early Paleozoic rifting followed by Late Paleozoic accretion. *Amer J Sci* 310: 523–574
- KRÖNER A, KOVACH V, ALEXEIEV D, WANG KL, WONG J, DEGTYAREV K, KOZAKOV I (2017) No excessive crustal growth in the Central Asian Orogenic Belt: further evidence from field relationships and isotopic data. *Gondwana Res* 50: 135–166
- LAURENT O, MARTIN H, MOYEN JF, DOUCELANCE R (2014) The diversity and evolution of late-Archean granitoids: evidence for the onset of 'modern-style' plate tectonics between 3.0 and 2.5 Ga. *Lithos* 205: 208–235
- LEHMANN J, SCHULMANN K, LEXA O, CORSINI M, KRÖNER A, ŠTÍPSKÁ P, TOMURHUU D, OTGONBATOR D (2010) Structural constraints on the evolution of the Central Asian Orogenic Belt in SW Mongolia. *Amer J Sci* 310: 575–628
- LEHMANN J, SCHULMANN K, LEXA O, ZÁVADA P, ŠTÍPSKÁ P, HASALOVÁ P, BELYANIN G, CORSINI M (2017) Detachment folding of partially molten crust in accretionary orogens: a new magma-enhanced vertical mass and heat transfer mechanism. *Lithosphere* 9: 889–909
- LONG XP, SUN M, YUAN C, XIAO WJ, LIN SF, WU FY, XIA XP, CAI K (2007) Detrital zircon age and Hf isotopic studies for metasedimentary rocks from the Chinese Altai: implications for the Early Paleozoic tectonic evolution of the Central Asian Orogenic Belt. *Tectonics* 26: TC5015
- LONG XP, LUO J, SUN M, WANG XC, WANG YJ, YUAN C, JIANG YD (2019) Detrital zircon U–Pb ages and whole-rock geochemistry of early Paleozoic metasedimentary rocks in the Mongolian Altai: insights into the tectonic affinity of the whole Altai-Mongolian Terrane. *GSA Bull* 132: 477–494
- MARKOVA NG (1975) Stratigraphy of the Lower and Middle Paleozoic of western Mongolia. In: *Transactions of Joint Soviet-Mongolian Scientific Research Geological Expedition* 12: 119. Nauka Press, Moscow (in Russian)

- MOSSAKOVSKY AA, DEGRUNOV AB (1985) The Caledonides of Kazakhstan, Siberia and Mongolia: a review of structure, development history and palaeotectonic environments. In: GEE DE, STURT BA (eds) *The Caledonide Orogen: Scandinavia and Related Areas*. John Wiley and Sons, Chichester, pp 1201–1215
- MOSSAKOVSKY AA, RUZHENTSEV S V, SAMYGIN SG, KHERASKOVA TN (1993) The Central Asian fold-belt: geodynamic evolution and the history of formation. *Geotectonics* 6: 3–31 (in Russian)
- NGUYEN H, HANŽL P, JANOUŠEK V, SCHULMANN K, ULRICH M, JIANG YD, LEXA O, ALTANBAATAR B, DEILLER P (2018) Geochemistry and geochronology of Mississippian volcanic rocks from SW Mongolia: implications for terrane subdivision and magmatic arc activity in the Trans-Altai Zone. *J Asian Earth Sci* 164: 322–343
- PATON C, HELLSTROM J, PAUL B, WOODHEAD J, HERGT J (2011) Iolite: freeware for the visualisation and processing of mass spectrometric data. *J Anal At Spectrom* 26: 2508–2518
- PEARCE JA, (1996) Sources and settings of granitic rocks. *Episodes* 19: 120–125
- PEARCE JA, PEATE DW (1995) Tectonic implications of the composition of volcanic arc magmas. *Annu Rev Earth Planet Sci* 23: 251–285
- PEARCE JA, HARRIS NBW, TINDLE AG (1984) Trace element discrimination diagrams for the tectonic interpretation of granitic rocks. *J Petrol* 25: 956–983
- PEARCE JA, STERN RJ, BLOOMER SH, FRYER P (2005) Geochemical mapping of the Mariana arc-basin system: implications for the nature and distribution of subduction components. *Geochem Geophys Geosyst* 6: Q07006
- PECCERILLO A, TAYLOR SR (1976) Geochemistry of Eocene calc-alkaline volcanic rocks from the Kastamonu area, northern Turkey. *Contrib Mineral Petrol* 68: 61–81
- RAUZER AA, ZHANCHIV DI, GOLYAKOV VI, YKHINA IF, IVANOV IG, TSUKERNIK AB, AFONIN V V, SMIRNOV IG, BYKHOVER VI, KRAVTSSEV A V, BAATARKHUYAG A, SKORYUKIN MI, KHODIKOV I V, MANTSEV N V, OKAEMOV S V, MISCHIN VA, ENKHSAJKHAN T, RAUZER AA, ŽANČIV DI, GOLYAKOV VI, YKHINA IF, IVANOV IG, TSUKERNIK AB, AFONIN V V, SMIRNOV IG, BYKHOVER VI, KRAVTSSEV A V, BAATARKHUYAG A, SKORYUKIN MI, KHODIKOV I V, MANTSEV N V, OKAEMOV S V, MISCHIN VA, ENKHSAJKHAN T (1987) Report on Results of Geological Survey at a Scale of 1 : 200,000, Performed in Southeastern Part of the Mongolian Altai, Mongolian National Republic in 1983–1986. Tekhnoexport, Moscow (in Russian)
- RUZHENTSEV S V, POSPELOV II (1992) The South-Mongolian Variscan fold system. *Geotektonika* 5: 45–62 (in Russian)
- RUZHENTSEV SV, BADARCH G, VOZNESENSKAYA TA (1985) Tectonics of Trans-Altai Zone of Mongolia. *Geotektonika* 4: 28–40 (in Russian)
- SAUNDERS AD, NORRY MJ, TARNEY J (1991) Fluid influence on the trace element compositions of subduction zone magmas. In: TARNEY J, PICKERING KT, KNIPE RJ, DEWEY JF (eds) *The Behaviour and Influence of Fluids in Subduction Zones*. The Royal Society, London, pp 151–166
- SCHANDL ES, GORTON MP (2002) Application of high field strength elements to discriminate tectonic settings in VMS environments. *Econ Geol* 97: 629–642
- SHAND SJ (1943) *Eruptive Rocks. Their Genesis, Composition, Classification, and Their Relation to Ore-Deposits with a Chapter on Meteorite*, 2nd edition. John Wiley & Sons, New York, pp 1–444
- SLÁMA J, KOŠLER J, CONDON DJ, CROWLEY JL, GERDES A, HANCHAR JM, HORSTWOOD MSA, MORRIS GA, NASDALA L, NORBERG N, SCHALTEGGER U, SCHOENE B, TUBRETT MN, WHITEHOUSE MJ (2008) Plešovice zircon – a new natural reference material for U–Pb and Hf isotopic microanalysis. *Chem Geol* 249: 1–35
- SOEJONO I, BURIÁNEK D, SVOJTKA M, ŽÁČEK V, ČÁP P, JANOUŠEK V (2016) Mid-Ordovician and late Devonian magmatism in the Togtokhinshil Complex: new insight into the formation and accretionary evolution of the Lake Zone (western Mongolia). *J Geosci* 61: 5–23
- SOEJONO I, BURIÁNEK D, JANOUŠEK V, SVOJTKA M, ČÁP P, ERBAN V, GANPUREV N (2017) A reworked Lake Zone margin: chronological and geochemical constraints from the Ordovician arc-related basement of the Hovd Zone (western Mongolia). *Lithos* 294–295: 112–132
- SOEJONO I, PEŘESTÝ V, SCHULMANN K, ČOPJAKOVÁ R, SVOJTKA M, ŠTÍPSKÁ P, BURIÁNEK D, JANOUŠEK V, LEXA O (2021) Structural, metamorphic and geochronological constraints on Palaeozoic multi-stage geodynamic evolution of the Altai accretionary wedge system (Hovd Zone, western Mongolia). *Lithos* 396–397: 106204
- SONG P, WANG T, TONG Y, ZHANG J, HUANG H, QIN Q (2019) Contrasting deep crustal compositions between the Altai and East Junggar orogens, SW Central Asian Orogenic Belt: evidence from zircon Hf isotopic mapping. *Lithos* 328–329: 297–311
- SUKHBAATAR T, LEXA O, SCHULMANN K, AGUILAR C, ŠTÍPSKÁ P, WONG J, JIANG YD, MÍKOVÁ J, ZHAO D (2022) Paleozoic geodynamics and architecture of the southern part of the Mongolian Altai Zone. *Tectonics* 41: e2022TC007498
- SUN SS, McDONOUGH WF (1989) Chemical and isotopic systematics of oceanic basalts: implications for mantle composition and processes. In: SAUNDERS AD, NORRY MJ (eds) *Magmatism in Ocean Basins*. Geological Society of London Special Publications 42, pp 313–345
- SUN M, YUAN C, XIAO WJ, LONG XP, XIA XP, ZHAO GC, LIN SF, WU, FY, KRÖNER A (2008) Zircon U–Pb and Hf isotopic study of gneissic rocks from the Chinese Altai: progressive accretionary history in the early to middle Palaeozoic. *Chem Geol* 247: 352–383

- ŞENGÖR AMC, NATAL'IN BA, BURTMAN VS (1993) Evolution of the Altiid tectonic collage and Palaeozoic crustal growth in Eurasia. *Nature* 364: 299–307
- TATSUMI Y, EGGINS S (1995) Subduction Zone Magmatism. *Frontiers in Earth Sciences*, Blackwell, Cambridge, Mass., pp 1–211
- TOMURTOGOO O (2014) Tectonics of Mongolia. Tectonics of Northern, Central, and Eastern Asia, Explanatory Note to the Tectonic Map of Northern Central Eastern Asia and Adjacent Areas at Scale 1 : 2,500,000. VSEGEI, Saint Petersburg, pp 110–126
- TOMURTOGOO O (2017) Tectonic map of Mongolia, scale 1 : 3,000,000 (with brief explanatory legend on the map in Mongolian). Geological Information Centre MRPAM, Ulaanbaatar
- TONG Y, WANG T, SIEBEL W, HONG DW, SUN M (2012) Recognition of early Carboniferous alkaline granite in the southern Altai Orogen: post-orogenic processes constrained by U–Pb zircon ages, Nd isotopes, and geochemical data. *Int J Earth Sci* 101: 937–950
- TONG Y, WANG T, JAHN BM, SUN M, HONG DW, GAO JF (2014) Post-accretionary Permian granitoids in the Chinese Altai Orogen: geochronology, petrogenesis and tectonic implications. *Amer J Sci* 314: 80–109
- VERMEESCH P (2018) IsoplotR: a free and open toolbox for geochronology. *Geosci Front* 9: 1479–1493
- VORONTSOV AA, PERFILOVA OY, KRUK NN, TARASYUK AS (2019) Late Ordovician volcanism of the northern part of Altai–Sayan area and its geodynamic nature. *Dokl Acad Sci* 485:457–463 (in Russian)
- WANG T, HONG DW, JAHN BM, TONG Y, WANG YB, HAN BF, WANG XX (2006) Timing, petrogenesis, and setting of Paleozoic synorogenic intrusions from the Altai Mountains, northwest China: implications for the tectonic evolution of an accretionary orogen. *J Geol* 114: 735–751
- WIEDENBECK M, ALLÉ P, CORFU F, GRIFFIN WL, MEIER M, OBERLI F, VON QUADT A, RODDICK JC, SPIEGEL W (1995) Three natural zircon standards for U–Th–Pb, Lu–Hf, trace element and REE analyses. *Geostand Newsl* 19: 1–23
- WINCHESTER JA, FLOYD PA (1977) Geochemical discrimination of different magma series and their differentiation products using immobile elements. *Chem Geol* 20: 325–343
- WINDLEY BF, ALEXEIEV D, XIAO WJ, KRÖNER A, BADARCH G (2007) Tectonic models for accretion of the Central Asian Orogenic Belt. *J Geol Soc London* 164: 31–47
- XIAO WJ, WINDLEY BF, BADARCH G, SUN S, LI J, QIN K, WANG Z (2004) Palaeozoic accretionary and convergent tectonics of the southern Altaiids: implications for the growth of Central Asia. *J Geol Soc London* 161: 339–342
- XIAO WJ, WINDLEY BF, HUANG BC, HAN CM, YUAN C, CHEN HL, SUN M, SUN S, LI JL (2009) End-Permian to mid-Triassic termination of the accretionary processes of the southern Altaiids: implications for the geodynamic evolution, Phanerozoic continental growth, and metallogeny of Central Asia. *Int J Earth Sci* 98:1189–1217
- XIAO WJ, WINDLEY BF, SUN S, LI JL, HUANG B, HAN CM, YUAN C, SUN M, CHEN HL (2015) A tale of amalgamation of three Permo–Triassic collage systems in Central Asia: oroclinal sutures, and terminal accretion. *Annu Rev Earth Planet Sci* 43: 477–507
- XIAO WJ, WINDLEY BF, HAN CM, LIU W, WAN B, ZHANG J, AO SJ, ZHANG ZY, SONG DF (2018) Late Paleozoic to early Triassic multiple roll-back and oroclinal bending of the Mongolia collage in Central Asia. *Earth-Sci Rev* 186: 94–128
- YUAN C, SUN M, XIAO WJ, LI XH, CHEN HL, LIN SF, XIA XP, LONG XP (2007) Accretionary orogenesis of the Chinese Altai: insights from Paleozoic granitoids. *Chem Geol* 242: 22–39
- ZHANG C, LIU LF, SANTOSH M, LUO Q, ZHANG X (2017a) Sediment recycling and crustal growth in the Central Asian Orogenic Belt: evidence from Sr–Nd–Hf isotopes and trace elements in granitoids of the Chinese Altay. *Gondwana Res* 47: 142–160
- ZHANG JJ, WANG T, TONG Y, ZHANG ZC, SONG P, ZHANG L, HUANG H, GUO L, HOU Z (2017b) Tracking deep ancient crustal components by xenocrystic/inherited zircons of Palaeozoic felsic igneous rocks from the Altai–East Junggar Terrane and adjacent regions, western Central Asian Orogenic Belt and its tectonic significance. *Int Geol Rev* 59: 2021–2040
- ZONENSHAIN LP (1973) The evolution of Central Asiatic geosynclines through sea-floor spreading. *Tectonophysics* 19: 213–232